

Fracture and interfacial delamination origins of bilayer ceramic composites for dental restorations

Yihong Liu^a, Hailan Feng^a, Yiwang Bao^b, Yan Qiu^b, Ning Xing^c, Zhijian Shen^{d,*}

^a School and Hospital of Stomatology, Peking University, 100081 Beijing, China

^b China Building Material Tests and Certification Centre, China Building Materials Academy, 100024 Beijing, China

^c China National Building Material Group Corporation, 100044 Beijing, China

^d Department of Inorganic Chemistry, Arrhenius Laboratory, Stockholm University, 10691 Stockholm, Sweden

Received 5 August 2009; received in revised form 9 November 2009; accepted 26 November 2009

Available online 22 December 2009

Abstract

Alumina and zirconia (Y-TZP) based bilayer ceramic dental composites with core to veneer thickness ratio (*R*-value) of 1:1 and 2:1 were fabricated through an established dental laboratory multi-steps-firing procedure. Their flexural strengths were determined by three-point bending test. A combinational approach of numerical simulations by finite element analysis associated with direct fractography investigation was applied to elucidate the origins of fracture and interfacial delamination and the influence of physical properties mismatch between core ceramic and veneer porcelain. A newly developed argon ion beam cross-section polishing technique was used to conduct fine polishing required for close investigating of the core–veneer interface under scanning electron microscope. For the same core ceramic no significant difference was observed in determined flexural strength of two groups of bilayer composites. The flexural strength of the bilayer composites is ~55% and ~35% of the core ceramics and achieved ~90% and 70–77% of the predicated value respectively in case of Y-TZP and alumina based composites. Numerical simulations by finite element analysis indicate that the often observed interfacial delamination in Y-TZP based bilayer composites has a clear origin of the severe physical properties mismatch between veneer porcelain and core ceramics, particularly the flexural strength, which may be prevented by increasing the flexural strength of veneer porcelain to above 300 MPa. The observation of the formation of microcracks in alumina core immediately one grain-thick under the veneer–core interface warns the possible thermal damages initiated during the veneering operation.

© 2009 Elsevier Ltd. All rights reserved.

Keywords: Composites; Failure analysis; Interfaces; Strength; Biomedical applications

1. Introduction

State of the arts all-ceramic dental restorations are dome-like structures composed of two layers of materials, namely the reinforcing ceramic core for bearing the biting load and the veneer porcelain for aesthetics. This materials solution is widely applied in dentistry owing to the excellent aesthetics and biocompatibility it provides. To further improve the reliability and durability of ceramic restorations, besides the commonly used alumina, glass infiltrated alumina and glass–ceramics, tetragonal zirconia polycrystalline ceramics (Y-TZP), a family of tough ceramics initially developed for engineering applications, have been increasingly adopted for core materials. In this case, a new

type of fracture mode emerged, known as veneer flaking. Earlier the cracks were often observed to pass straight across the veneer–core interface in dental crowns when alumina or glass infiltrated alumina or glass–ceramics was used as the core material. This results in the crack of entire crown that is commonly called crown cracking for short in clinic.^{1,2}

In general, two major factors affect the fracture behaviours, namely (i) the interfacial bonding between the core and veneer materials. Thus, chemical mismatch and poor wetting of the core by the veneer porcelain may cause inferior core–veneer bond strength,³ and (ii) the mismatch of the physical properties of core ceramic and veneer porcelain. The coefficient of thermal expansion (CTE) mismatch results, for instance, residual stresses when cooling from the preparation temperature of the veneering porcelain, typically being between 900 and 1000 °C.^{4–7} In clinic, the thickness of the veneer porcelain is never even and the veneer layer is build-up by a manual multi-steps-firing proce-

* Corresponding author. Tel.: +46 08 162388; fax: +46 08 152187.
E-mail address: shen@inorg.su.se (Z. Shen).

ture. This increases the complexity of stress distribution, which becomes difficult to study if a simplified model would not be introduced. The evenly thick flat bilayer ceramic composite specimens were, therefore, developed to simulate the fracture behaviours. Accordingly, it has been revealed that the fracture resistance and failure modes of bilayer ceramic composite specimens were dependent on the core to veneer thickness ratio,^{8–10} and were influenced by surface treatments and surface defects,¹¹ as well as by testing and loading methodologies.^{9,12} The interfacial delamination has been ascribed to large mismatch of the fracture toughness¹³ or the fracture toughness and elastic modulus.¹⁴

As the bilayer ceramic composite comprise two layers of ceramics with very different mechanical performances, it is of outmost importance to identify the crack origin and the crack propagating trajectory for understanding the fracture mechanism(s) and for improving the performances of dental restorations. During mechanical testing the fracture of bilayer all-ceramic specimens occurs instantly when a critical stress is reached, which makes it impossible to follow the evolution of propagating cracks. One way to overcome this drawback is to use numerical simulations by finite element analysis (FEA). This technique has been applied to facilitate analyses of stress distributions during simulated mechanical loadings of dental restorations.^{15,16}

In the present work, rectangular platelet bilayer ceramic composite specimens consisting of alumina and respectively Y-TZP as ceramic cores and silicate based glasses as veneer porcelains were produced according to an established dental laboratory multi-steps-firing procedure. Their bending strengths were tested, following with detailed fractography investigation by optical and electron microscopes. FEA method was employed to simulate the crack initiation, crack propagation and fragmentation or delamination processes during the fracture of the bilayer composites with test bar geometries used for the 3-point bending test. Our aim is to, through a combinational approach of experimental tests and numerical simulations, define the fracture and delamination origins thus to guide the restorations design and the materials development suited for this rapidly growing medical application of structural ceramics.

2. Experimental procedures

2.1. Materials preparation

Dense ceramic blocks were made of high purity alumina and 3 mol% yttria stabilized Y-TZP, respectively. The two ceramics were prepared by cold isostatic pressing (CIP) followed with pressure-less sintering (PLS) in air, *i.e.* in the same way as the industrial processes widely applied in dentistry. The rectangular testing bars were then prepared by cutting the blocks, followed by grinding and double-sides polishing. The surface of the test bar to be veneered by porcelain was finished by sandblasting with 25 μm aluminium oxide abrasive under 0.4 MPa of pressure at a distance about 10 cm. The samples were faced to the sand beam with an angle of 45° with sandblasting time about 1 min. Y-TZP and alumina core bars were veneered individually with

commercial veneer porcelains developed for Y-TZP or alumina (Rondo, Nobel Biocare AB, Gothenburg, Sweden). Alumina core bars were veneered with another type of porcelain (Vintage for Alumina, SHOFU Dental Co., Japan). In order to reflect the possible impact of the veneering process on mechanical properties, the bilayer specimens were prepared strictly according to the recommended dental laboratory multi-steps-firing procedure for each porcelain and ceramic. These procedures are specially developed for making all-ceramic crowns with several veneer firing steps interposed by rapid heating and cooling. During the first firing cycle a veneer layer with approximate target-thickness was built-up and fired. At least one more correction firing cycle was then conducted to compensate for the sintering shrinkage of veneer layer in order to achieve exactly the right dimensions. Considering the possible introduction of cracks on core surface by sandblasting before veneering and in order to test the influence of thermal mismatch between core and veneer materials, additional alumina based bilayer specimens individually veneered with Rondo and Vintage, respectively, were prepared by sand paper grinding of the core material surface instead of sandblasting.

2.2. Three-point bending test

The core ceramic bars without veneering have standard dimensions, *i.e.* 20 mm in long, 4 mm in wide, and 1.2 mm in height. Single alumina and Y-TZP ceramic bars were tested as control groups. The veneered test bars with two different ratios of core to porcelain thickness, referred as *R*-value below, were tested yielding bilayer specimens with two different test bar thicknesses. These are Group 1:1 samples (*R* = 1, 20 mm in length, 4 mm in width, and 2.4 mm in height) and Group 2:1 samples (*R* = 2, 20 mm in length, 4 mm in width, and 1.8 mm in height). Each group of the bending test composed of 10 test bars. The test bars were ground on both top and bottom surfaces with first a 100-grit and then by a 150-grit Al₂O₃ abrasive paper. One surface to be placed opposite the load in the test rig received additional polishing by use of a sequence of steps that ranged from 180-grit to 600-grit SiC abrasive papers and for the bilayer bars this was done on the core ceramic surface. The cross-sectional dimension of each specimen was carefully controlled by a micrometer.

Three-points bending test was performed in accordance with ISO 6872:1995(E) standard for dental ceramics. Flexural strength of all specimens was evaluated on the universal test machine (CMT5105, Sansi Co., China) with a testing bar span of 15 mm. The load was applied on the centre of the veneer surface and the crosshead speed is 0.5 mm/min. The apparent flexural strength (σ_f) of the bilayer composite beams was calculated by the following equation:

$$\sigma_f = \frac{3PL}{2bd^2} \quad (1)$$

where *P* is the fracture load; *L* is the span; *b* is the width of the specimen; *d* is the thickness of the specimen. Multiple comparisons of the mean flexure strength of the core ceramics, and bilayer composite specimens were performed using the one-

Table 1
Mechanical properties of the materials used in the present numerical stimulation.

| Materials | Bending strength (MPa) | Young's modulus (GPa) | Poisson' ratio | Thermal expansion coefficient ($\times 10^{-6} \text{ K}^{-1}$) |
|--------------------------------|------------------------|-----------------------|--------------------|---|
| Alumina | 690 ^a | 380 ^a | 0.22 ¹⁹ | 8.0 ^a |
| Rondo porcelain for alumina | 120 ^a | 85.8 ¹⁹ | 0.22 ¹⁹ | 7.0 ^a |
| Vintage porcelain for alumina | 94 ²⁰ | 65 ²⁰ | 0.22 ¹⁹ | 6.7 ^a |
| Y-TZP | 1121 ^a | 210 ^a | 0.29 ¹⁹ | 10.4 ^a |
| Rondo porcelain for Y-TZP | 120 ^a | 85.8 ¹⁹ | 0.22 ¹⁹ | 9.3 ^a |
| Si ₃ N ₄ | 2108 ²¹ | 304 ²² | 0.24 ²² | 16.0 ¹⁹ |

^a Data provide by the manufactures.

way analysis of variance (ANOVA) and Tukey's post hoc test ($p < 0.05$) by SPSS 10.0 software (SPSS Inc., Chicago, IL, USA). The apparent flexural strength of the bilayer composite beams depends on the strength of the two individual layers and the ratio of their elastic modulus, see [Appendix A](#).

2.3. Finite element analysis

The numerical FEA program RFPA'2D (Rock Failure Process Analysis, Northeast University, China) is an appropriate tool for simulating and studying the fracture processes of brittle materials.^{17,18} In present study, the RFPA'2D was utilized to analyse the fracture process of the veneered alumina and Y-TZP bilayer composite specimens with *R*-value of 1 and 2. The numerical simulation of the loading was simplified to strain in two-dimensions, *i.e.* a plane parallel to the load force direction. The geometry of the test volume was similar to the ceramic bars used in the 3-point bending test (20 mm long, 4 mm wide, 1.2 mm core height, 1.2 or 0.6 mm porcelain height). The mechanical properties of the ceramics used in the calculations and those of the Si₃N₄ sustainers of 3-point bending test are summarized in [Table 1](#).

The models were divided into 480×90 elements and 480×72 elements for the Group 1:1 and the Group 2:1 configuration, respectively. The loading point was applied in the centre of the veneer surface at the top of the bilayer bar and a displacement load with increment of 0.02 mm per step was used. The fracture process was modelled step-by-step and smaller loads were applied in the interval where element failure occurred within one of the original loading steps. Hooke's law was applied to describe the relationship between stress and strain until failure occurred, *i.e.* the framework deformed linearly and elastically. The interface between core and veneer was assumed to bind coherently and the residual stress caused by CTE mismatch between core and veneer was neglected.

Acoustic emissions (AE) are the stress waves induced by the sudden internal stress redistribution of the materials caused by the change in the internal structure during stress. In RFPA'2D calculations it was assumed that the strain energies released by damage elements were all in the form of AE. The AE energy was mathematically calculated in RFPA'2D by

$$\Delta e_i = e_{ic} - e_{ir} \quad (2)$$

where e_{ic} was the elemental strain energy of element "i" before failure, e_{ir} was its strain energy after failure. The elemental strain

energy depended on the elastic modulus of the element, the stresses before and after failure, and the volume of the element.¹⁶

Alumina models in Group R1 were calculated where the veneer porcelain' flexural strength of 120 MPa were stepwise lowered to 100, 90, 80, 70, 60 and 50 MPa. Similarly, Y-TZP models in Group R1 were calculated by increasing veneer porcelain' flexural strength stepwise to 180, 240, 300 and 360 MPa. For both alumina and Y-TZP models in Group R2 only a declined veneer porcelain' flexural strength of 70 MPa was calculated.

2.4. Microstructure characterization

Fractured pieces of each bilayer specimen were collected after the bending test and studied with an optical microscope (Motic k400, Preiser Scientific, Louisville, KY, USA) to examine the features of the fracture surface. High resolution fractography investigations were carried out by using a field emission Scanning Electron Microscope (SEM, JEOL JSM-7000F, Jeol Ltd., Tokyo, Japan). For analysing the core to veneer interface one beam each of Group 1:1 specimen for both Y-TZP and alumina was prepared for SEM observation after polishing the cross-sections by using an argon ion milling system (JEOL SM-09010 cross-section polisher) operated at 5 kV/90 μ A. The polishing time was set to 15 h. Using this way of extremely gentle polishing any possible damages that might be introduced by using common mechanical polishing is minimized.

3. Results

3.1. The flexural strength and fractography

The three-points bending test results for each group of bilayer specimens are summarized in [Table 2](#). The mean apparent flexural strength (σ_f) of bilayer ceramic composites was significantly ($p < 0.05$) lower than that of the corresponding core ceramics, *i.e.* $\sim 35\%$ and $\sim 55\%$ of the strength of the core material for alumina and Y-TZP bilayer specimens, respectively. No major differences were found between the two groups of bilayer specimens with *R* equalling of 1 and 2 ($p > 0.05$). In general, the apparent flexural strengths of bilayer Y-TZP specimens were more than three times higher than that of bilayer alumina specimens ($p < 0.05$) and even higher than the pure alumina core test bars. As shown in [Table 2](#), the measured apparent flexural strengths (σ_f) of the bilayer composite beams are lower than that predicted by the theoretical calculation, *i.e.* only $\sim 90\%$ and 70–77%

Table 2
Bending strengths measured by 3-points bending test and predicated according Eq. (4) in Appendix A.

| Group | Bending strength measured | | | | Bending strength predicated, ^a σ_b (MPa) | σ_f/σ_b | |
|-------------|---------------------------|------|------|-------------------------|--|---------------------|-------|
| | Mean, σ_f (MPa) | SD | SE | 95% confidence interval | | | |
| | | | | Lower | | | Upper |
| Alumina | 514 | 20.4 | 7.7 | 494.7 | 532.5 | | |
| Alumina 1:1 | 171a | 14.2 | 5.3 | 158.1 | 184.3 | 221 | 77% |
| Alumina 2:1 | 184a | 17.7 | 6.7 | 167.2 | 200.0 | 261 | 71% |
| Y-TZP | 1102 | 45.7 | 18.6 | 1053.9 | 1149.8 | | |
| Y-TZP 1:1 | 605b | 31.0 | 12.6 | 572.5 | 637.5 | 674 | 90% |
| Y-TZP 2:1 | 630b | 35.7 | 14.6 | 593.1 | 667.9 | 717 | 88% |

The values labelled with same letter (a and b) have no statistical different ($p > 0.05$).

^a The bending strength of 514 and 1102 MPa for alumina and Y-TZP, respectively, and Young's modulus of 380, 210 and 85.8 GPa for alumina, Y-TZP and procelian, respectively, were used to calculate the σ_b according Eq. (4) in Appendix A, assuming no damage of mechanical properties of each individual layer to occur during the veneering process.

of the predicated strength (σ_s) was achieved respectively in case of Y-TZP and alumina based composites.

The test bar specimens gave two major fracture pieces after the bending test and the fracture origin always located at the bottom surface in the middle between the support cylinders. In addition, delamination was observed in all bilayer Y-TZP specimens with almost completed physical separation of the veneer porcelain from the Y-TZP core material, but no similar extensive delamination was ever found in any of the alumina bilayer specimens, *cf.* Fig. 1a and b. In the latter case partial delamination occurred occasionally and covered only a small area very close to the fracture path through bilayer test bar. The typically observed fracture pieces of broken Y-TZP and alumina bilayer specimens as seen by optical microscopy are shown in Fig. 1. The location of the initial fracture point sim-

ulated by FEA calculation is shown below in the same figure for comparison. By high resolution SEM it was observed that the remaining porcelain fragments still stuck to the surface of the Y-TZP core appeared as small droplet-like islands, *cf.* Fig. 2a. Distinct stress fringes are observed inside the veneer porcelain. For alumina bilayer specimens, porcelain still stuck to the surface of the alumina core, whereas in limited area delamination was observed where occasionally some alumina grains were peeled-off in one grain-thick layer, *cf.* Fig. 2b. Good interfacial bonding was observed with stress fringes appearing to be concentrated in the interface region, see Fig. 2c, and microcracks were observed in the alumina core just below the veneer–alumina interface, *cf.* Fig. 2c. This microcracking appears to extend, in most cases, only one grain-thick into the alumina core.

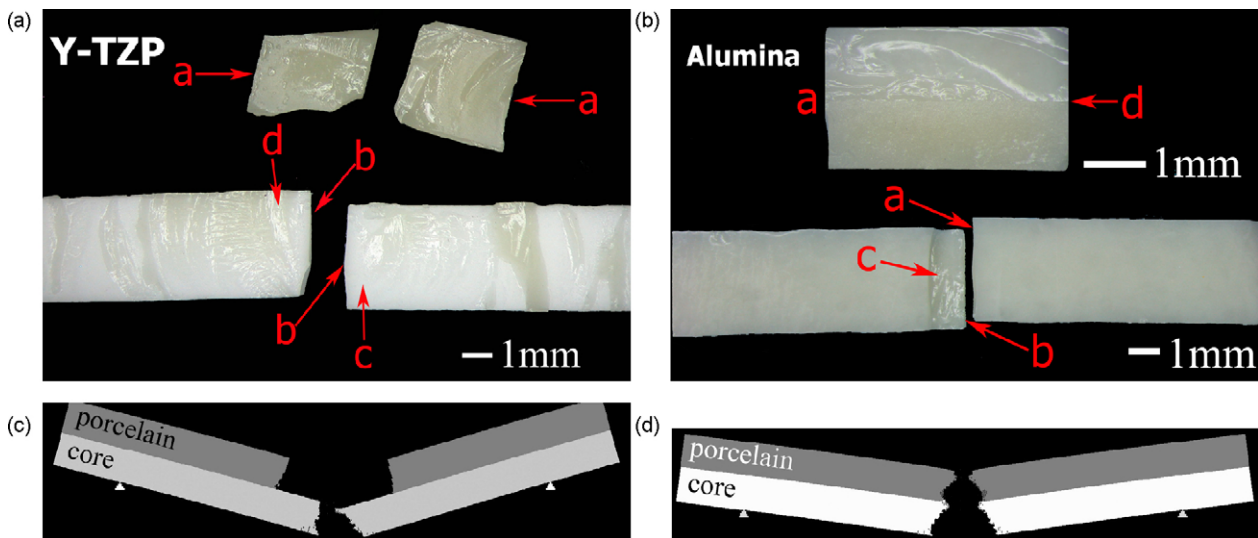


Fig. 1. The optical microscope view of the fractured bilayer specimens of Y-TZP (a) and alumina (b) after experimental 3-point bending test in comparison with the FEA simulated fracture features of the Y-TZP (c) and alumina (d) bilayer specimen (with $R = 1$). Note that the experimentally observed fracture features are in agreement with the FEA simulation results. In the case of Y-TZP bilayer composites (a) severe interfacial delamination was observed, where arrows “a” points to two pieces of veneer porcelain completely peeled-off from Y-TZP core; arrows “b” points to the location of fracture surfaces; arrow “c” indicates the Y-TZP core surface exposed by interfacial delamination; and arrow “d” indicates the veneer porcelain remaining on core interface. In the case of alumina bilayer composites (b) very limited interfacial delamination was observed, where arrows “a” and “b” indicate the location of fracture surfaces; arrow “c” indicates a small delamination zone; arrow “d” indicates the location of the veneer/core interface.

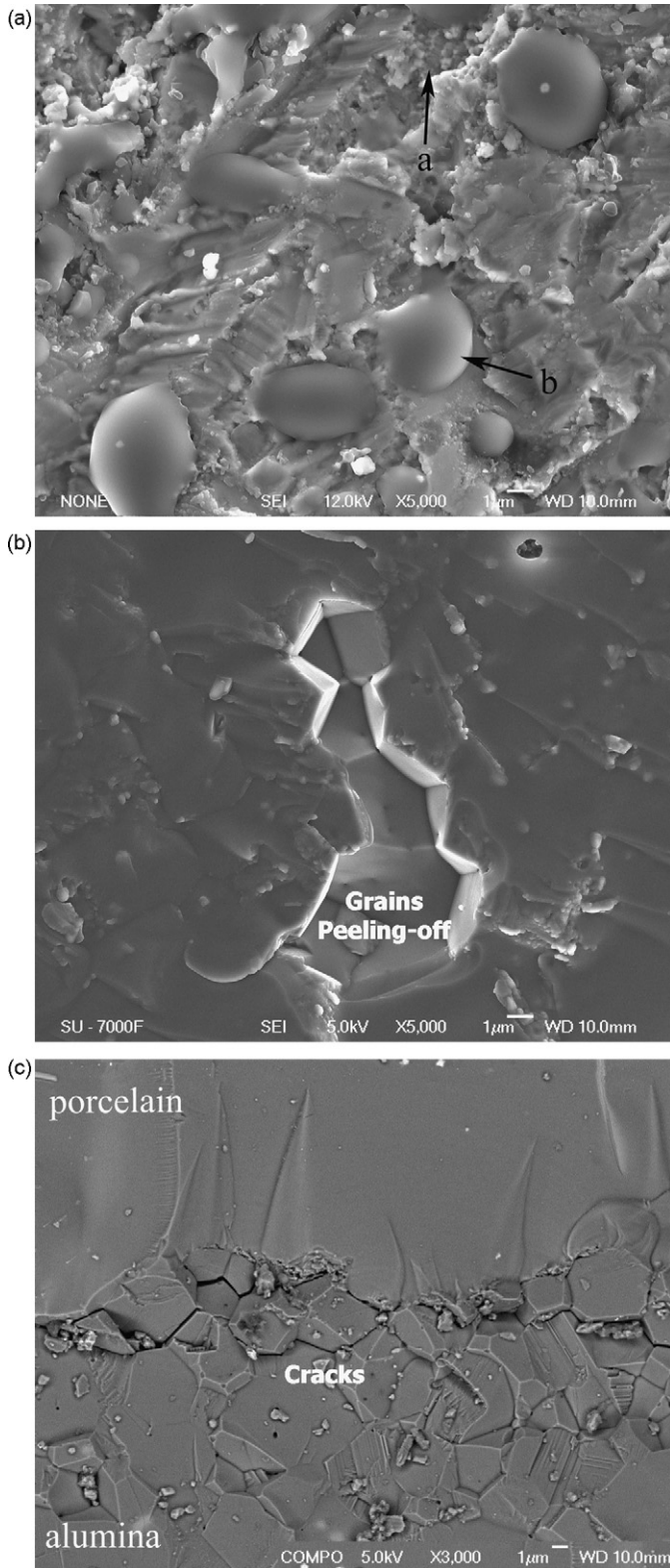


Fig. 2. The SEM images revealing the interface perpendicular to the fracture surface of a Y-TZP bilayer specimen after 3-point bending test, where arrows “a” indicate the Y-TZP grains exposed due to delamination and “b” the droplet-like veneer porcelain islands still sticking on the Y-TZP core (a); the SEM image of the fracture surface of an alumina bilayer specimen revealing the peeling-off a single grain layer of alumina grains under the veneer–alumina interface (b); and the SEM image of the fracture surface of an alumina bilayer specimen revealing the observation of microcracks one grain-thick under the interface and stress fringes presented in the veneer porcelain (c).

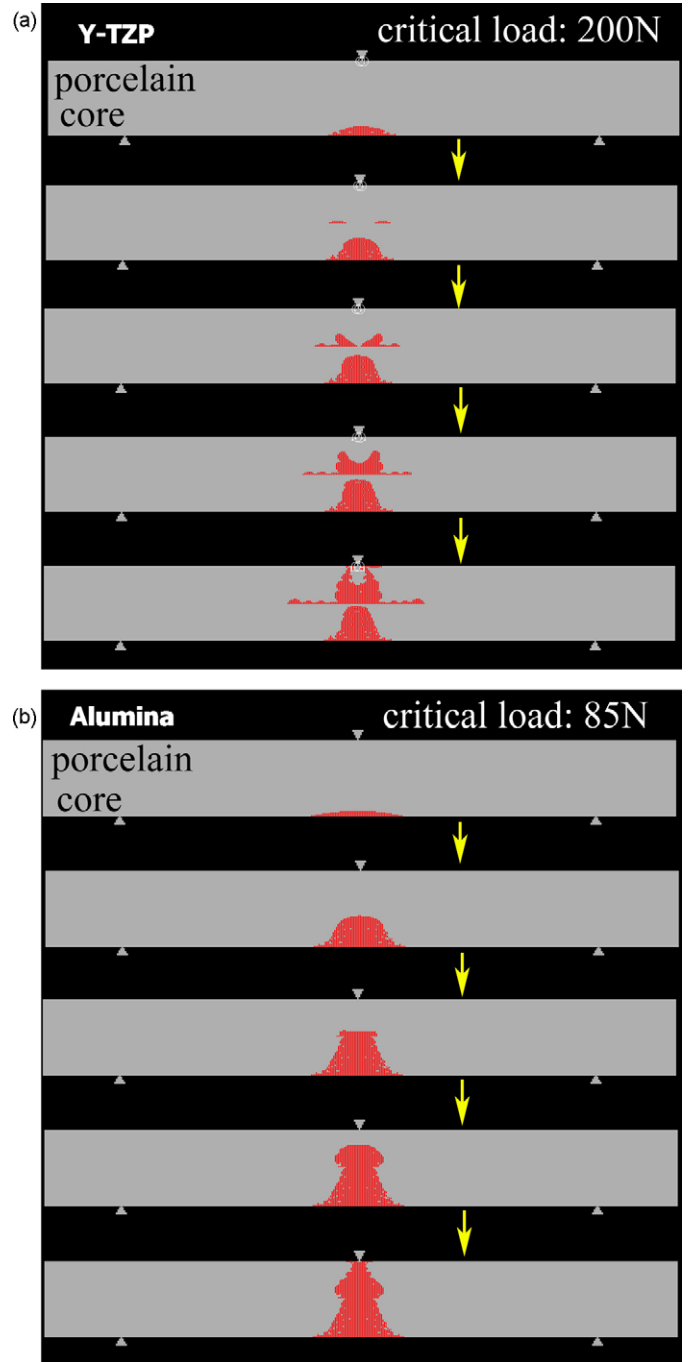


Fig. 3. AE maps revealing the initiation and propagation trajectory of cracks. In Y-TZP composite (a) the first crack is initiated on the core surface. When it propagates close to the core–veneer interface, another crack is initiated at interface leading to delamination. In alumina composite (b) the crack is initiated on the core surface and propagates straight through the interface with limited extension in perpendicular direction along the interface. Under three-point bending load the initial damage occurs at 200N and 85N for Y-TZP and alumina based bilayer specimens, respectively.

3.2. The crack origins and propagation trajectories

Acoustic emission stress waves calculated by FEA illustrate the initiation and propagation trajectories of cracks in two different composites, as illustrated in Fig. 3. The Y-TZP bilayer

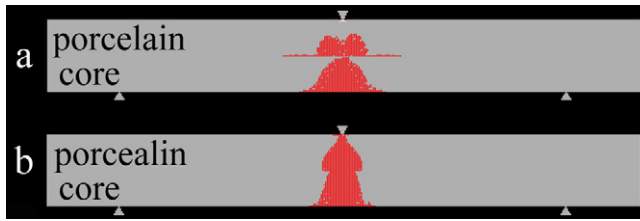


Fig. 4. AE maps revealing that fracture modes of bilayer composites change with the flexural strength of veneer porcelain. Interfacial delamination appears when the flexural strength of veneer porcelain is reduced to 70 MPa in alumina bilayer composites (a); delamination is avoided when the flexural strength of veneer porcelain is increased to 300 MPa in Y-TZP bilayer composites (b).

composite reveals an obvious stress build-up and delamination at the veneer–Y-TZP interface, see Fig. 3a. The fracture process of the alumina bilayer composite, on the other hand, proceeds with almost no delamination at the interfacial zone, as seen in Fig. 3b. It appears that the mismatch of the flexural strength of the two ceramics forming the bilayer composite is one of the mechanical factors that influence the crack path and sensitivity for delamination at the interface, as illustrated in Fig. 4. It is possible to achieve an interfacial delamination even with alumina as core material when the flexural strength of porcelain was declined to 70 MPa, see Fig. 4a. When the flexural strength of porcelain is set to values larger than 70 MPa, however, this strength has almost no influence on the overall strength of the bilayer composites. By contrast, in case of Y-TZP the interfacial delamination disappears when the flexural strength of porcelain is increased to 300 MPa, cf. Fig. 4b. Above 100 MPa the flexural strength of porcelain has almost no influence on the overall strength of the bilayer composites.

3.3. The formation of cracks in alumina core at short distance under the interface

Microcracks were observed in the alumina core material just one grain-thick under the porcelain–alumina interface on fracture surfaces, as revealed in Fig. 2c. In order to clarify if the observed microcracks are formed during the bending test or if the microcracks have formed already during veneering processing an unbent bilayer specimen was carefully polished by mechanical polishing followed with a final step of extremely gentle Argon ion beam cross-section polishing. Fig. 5 shows an SEM image taken on such polished surface. The presence of a high concentration of microcracks in the alumina core material about one grain-thick under the interface is obvious. It confirms that the microcracks are formed during veneering process. Similar crack formation phenomena were observed in alumina bilayer specimens veneered with either Rondo or Vintage porcelains, regardless if the alumina bar surface is sandblasted or gently ground by sand paper before the veneering procedure. In Y-TZP bilayer samples such cracks were never observed in the Y-TZP layer close to the interface after veneering.

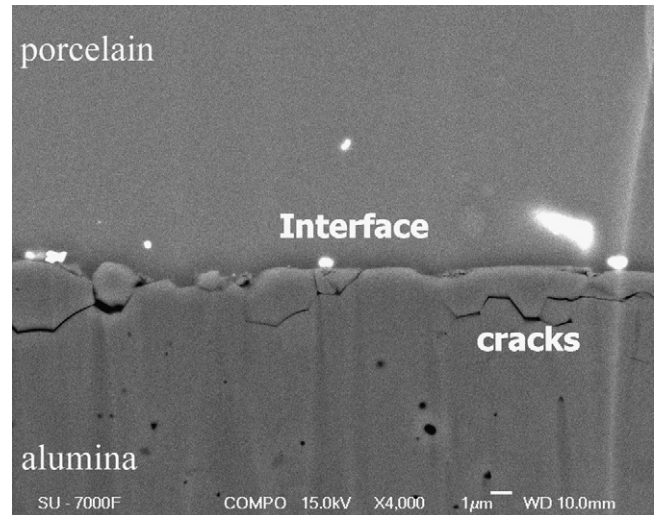


Fig. 5. An SEM image taken on Argon ion beam section polished surface revealing the formation of cracks in alumina core just on grain-thick below the interface between the core and veneer. In this case Rondo porcelain was used.

4. Discussions

4.1. The origins of interfacial delamination

In literature, the interfacial delamination has been ascribed either merely to the large mismatch of the fracture toughness¹³ or both to the fracture toughness and elastic modulus.¹⁴ In our FEA simulation the elastic modulus are involved but not fracture toughness as parameters of concern. Yet, the influence of fracture toughness is reflected by that of flexural strength, as the flexural strength is proportional to the fracture toughness, besides its determinable relation with the critical flow size of each specimen. The FEA simulation reveals that the interfacial delamination observed in Y-TZP bilayer composites is initiated by shear stresses building up along the interface due to the mechanical properties mismatch of the two constitutional ceramic components, especially the mismatch of flexural strength. It suggests that the delamination is possible to be avoided by increase the flexural strength of the veneer porcelain to above 300 MPa. A drastic increase of the flexural strength of veneer porcelain is thus a necessary step towards solving the problem of interfacial delamination, though technically it still remains a great challenge to achieve this.

The fracture in both alumina and Y-TZP bilayer composites were initiated by tension stresses, but the crack progressed in two different ways. The FEA simulations discussed above were carried out under the condition of one loading cycle, which means that even if the load was kept constant the crack continuously growth until complete failure of the composite material occurs. Thus, a bilayer ceramic composite is not “forgiving” once it starts to fracture. In the alumina case the failure went straight over the interface, whereas in the Y-TZP case an additional shear stress concentration was occurring at the interface, which made porcelain to start delaminating from Y-TZP just before the total failure. Y-TZP is still a better core material as the stress–strain curve showed that the critical loads for initiating a crack in the

Y-TZP were two times higher than that in alumina. By bearing mind the fact that interfacial delamination starts well before the crack propagates through the Y-TZP layer, one may understand that under the fatigue loading conditions local veneer flaking may occur, even though no critical damage of the Y-TZP core itself has taken place. We concluded that this is the main origin of the veneer flaking of Y-TZP crowns and bridges frequently observed in clinic.

One major assumption we made to simplify the calculation during FEA simulation is that the interface between core and veneer is coherent, and no influence the residual stress caused by thermal expansion coefficient mismatch between core and veneer is taken into account. As shown above, even under such an ideal load transfer condition interfacial delamination takes place when the flexural strength of veneer porcelain is below a critical value. In reality, the bonding between Y-TZP and veneer is never ideal. The presence of interfacial voids and the poor chemical bonding established between Y-TZP and silicate based veneer porcelain provides easy paths for cracks propagation along the interface. The interfacial delamination speeds up, particularly under the fatigue loading condition.

The experimental observation of stress fringes presented in the veneer porcelain reveals the built-up of residual thermal stresses in the veneer layer. The very smooth spherical morphology of the droplet-like veneer porcelain islands remaining on the Y-TZP surface after flaking further indicates a very high stress concentration inside the veneer porcelain bond onto the Y-TZP core. As in strengthened glass such high concentration of residual thermal stress encourages a dynamic breaking. In this case of Y-TZP bilayer composite, the flexural strength of Y-TZP is ten time higher than that of the veneer porcelain, which is high enough to initiate the process of dynamic breaking of the veneer layer.

4.2. The origins of unexpected low flexural strength of bilayerd composites

It is an unexpected observation that the bilayer composites, particularly the ones based on alumina, revealed lower apparent flexural strength (σ_f) than the predicated ones (σ_s). This low strength of alumina can hardly be interpreted unless a possible thermal damage of the core ceramic and its mechanical properties occur during the veneering process.

Previous studies have shown that the R -value influences on the stress distribution in bilayer composites. White et al. studied bilayer beams composed of thin core and thick veneer porcelain with tensile stress concentrated in the porcelain layer. They reported a declined failure load of the specimens¹⁰ and similar results were also reported by Fleming et al.⁸ Hsueh et al. analysed the influence of R -value on distribution of residual thermal stresses and on flexure strength determined by ring-on-ring loading method.²³ They found the location of maximum tension shifted from the porcelain surface to the In-ceram alumina/porcelain interface when the R -value changed from 0.5 to 1 and 2, and these calculations were confirmed by the observed trend of the failure origins in their experiments. It is of beneficial to build a compressive residual stresses in the porcelain layer

to discourage its failure. When the R -value equals 0.5 a tensile stress is built-up in porcelain and this is an undesired situation.²³ According our FEA stimulation, when residual thermal stress is not taken into account, very similar stress distribution and fracture mode is expected in bilayer composites with R -value equalling 1 and 2, in both cases of alumina and Y-TZP bilayer composites. However, the observations taken in our study shows that the thermal stresses in the case of an alumina core cannot be ignored and that the CTE match has to be better as well as the veneering procedures itself has to be considered to avoid extreme thermal shock.

The thermal mismatch between the core ceramic and veneer porcelain has been intensively discussed in the literature. For all-ceramic crowns of which all components are brittle, thermal stresses can be detrimental to both veneer and core. A close matching of the CTE was accordingly suggested to be highly desirable.²⁴ DeHoff et al. calculated the induced thermal stress supporting their experimental observation that a high residual thermal stress lead to failure of their specimens.⁶ A mismatch of $1 \times 10^{-6} \text{ K}^{-1}$ of CTE can yield thermal stresses in the order of 50 MPa within the layers.²⁵ In the present study, the CTE of veneer porcelain is set to be about $1 \times 10^{-6} \text{ K}^{-1}$ lower than that of the core ceramics for both alumina and Y-TZP bilayer composites aiming for establishing a compressive residual thermal stress in veneer layer whereas a balancing tensile residual thermal stress occur in the stronger core material. In this condition, the residual stresses have the maximum value at the porcelain–core interface which decreases with the distance from the interface.²³

The experimental observation of microcrack formation in the alumina core one grain-thick immediate below the interface is surprising to us. It reveals an issue that has not been well considered in the community, *i.e.* the possible thermal damages initiated during the veneering operation. In practice, the veneer porcelain layer on the ceramic coping is achieved by fusing porcelain onto the ceramic through a multi-steps-firing interposed by rapid heating and cooling. In order to mimic the components making procedure in this study we prepared all specimens strictly according this established dental laboratory routine. It appears that the tensile stress built-up in alumina core by a mismatch of $\sim 1 \times 10^{-6} \text{ K}^{-1}$ of CTE between core and porcelain is enough to initiate cracks in alumina core, that is usually thought to be strong enough to sustain a tensile thermal stress. An assumption of slow and homogeneous cooling is usually taken in calculating the residual stress built-up by CTE mismatch. This does obviously not reflect the existing dental laboratory procedure in which rapid cooling can easily lead to inhomogeneous complex thermal stress distribution. Under this consideration Y-TZP is more damage tolerant as we never observed any similar cracks in Y-TZP core.

5. Conclusions

Direct experimental tests showed that the flexural strength of the bilayer composites is $\sim 55\%$ and $\sim 35\%$ of the core ceramics and achieved $\sim 90\%$ and $70\text{--}77\%$ of the predicated value in case of Y-TZP and alumina based composites, respectively. For the

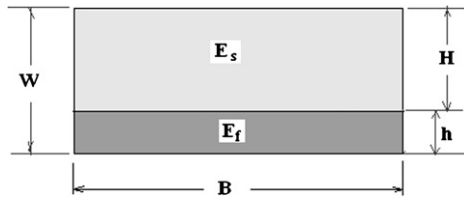


Fig. 6. A schematic view of the cross-section of a bilayer beam. E_s is the elastic modulus of the lower layer, E_f the modulus of the upper layer, B the width of the beam specimen, h the thickness of the up layer, H the thickness of the lower layer and W is the total thickness equalling $(h + H)$.

same core ceramic no significant difference is observed in determined flexural strength of two group bilayer composites with different core to veneer thickness ratios (with $R = 1$ and 2). FEA simulation revealed that the interfacial delamination in bilayer ceramic composites can be interpreted by the severe physical properties mismatch between core ceramic and veneer porcelain, particularly the flexural strength. It further predicates that the often observed delamination in Y-TZP bilayer composites might be avoided by increasing the flexural strength of veneer porcelain to 300 MPa. It is a surprising observation that the thermal stress generated by a CET mismatch of $\sim 1 \times 10^{-6} \text{ K}^{-1}$ between core and veneer porcelain is high enough to trigger microcracking in alumina core when porcelain layer is built-up by an established dental laboratory multi-steps-firing procedure. This warns the possible thermal damages initiated during the veneering operation.

Acknowledgement

This work was supported by the National Natural Science Foundation of China (project No. 50872003) and Swedish Science Council (VR) through its Research Link program. SEM studies were performed at the Electron Microscopy Centre at Arrhenius Laboratory, which is supported by the Knut and Alice Wallenberg foundation. The authors acknowledge T. Ekström for his helpful comments and X. Wang and D. Grüner for their technical supports.

Appendix A. Calculation of the ideal bending strength of a bilayer beam

For a flat bilayer beam with the cross-section geometry as sketched in Fig. 6, where B is the width of the beam, and H , h , and W represent the thickness of the upper layer, lower layer and the entire composite beam, respectively. Let the elastic modulus of the up layer (porcelain), lower layer (ceramic) and the entire composite beam to be E_s , E_f and E_c , respectively, and the ratio of modulus defined by

$$\alpha = \frac{E_f}{E_s} \quad (3)$$

The bending strength of the composite beam σ_b related to the strength of lower layer σ_f and the elastic modulus of both

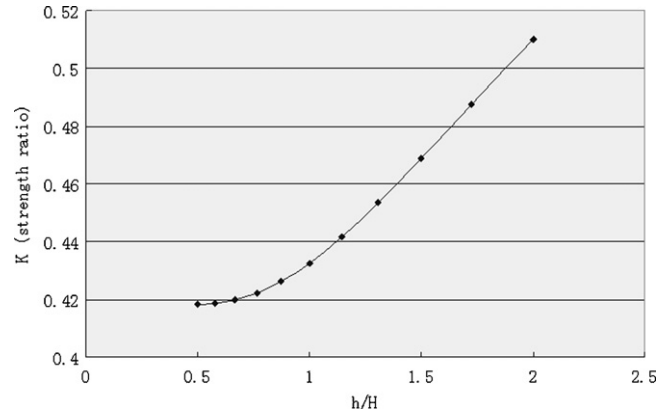


Fig. 7. The predicted strength parameter of the composite beam vs. the thickness ratio for the case of $\alpha = E_f/E_s = 350/80$ and when the total thickness is 3 mm and width of 4 mm.

layers:

$$\sigma_b = \frac{I}{\alpha I_b} \sigma_f = k \sigma_f \quad (4)$$

where

$$I_b = \frac{(B W^3)}{12} \quad (5)$$

and

$$I = I_1 = B \left\{ \frac{H^3}{12} + \frac{\alpha h^3}{12} + H \left[\frac{\alpha h(H+h)}{2(\alpha h + H)} \right]^2 + \alpha h \left[\frac{H^2 + Hh}{2(\alpha h + H)} \right]^2 \right\} A \quad (6)$$

k is determined by Eqs. (3), (5) and (6), i.e. it is related to the ratio of elastic modulus and geometric dimensions of the beam. The relationship between the thickness ratio and the k value is calculated and shown in Fig. 7. This is valid usually when $h/H < 1$. Corresponding calculation indicates: when the H -value is small, i.e. when the h -value is near the W value, the strength of composite beam should be close to the initial strength of the lower layer; when the elastic moduli of the two layers are the same, the strength of the composite beam equals the strength of the tensile (lower) layer; and when the thickness ratio is lower than 0.5, the strength ratio has very small variation.

References

1. Rekow D, Thompson VP. Near-surface damage—a persistent problem in crowns obtained by computer-aided design and manufacturing. *J Eng Med* 2005;**219**:233–43.
2. Steyern PV, Ebbesson S, Holmgren J, Haag P, Nilner K. Fracture strength of two oxide ceramic crown systems after cyclic pre-loading and thermo cycling. *J Oral Rehabil* 2006;**33**:682–9.
3. Aboushelib MN, Kleverlaan CJ, Feilzer AJ. Microtensile bond strength of different components of core veneered all-ceramic restorations. Part II: Zirconia veneering ceramics. *Dent Mater* 2006;**22**:857–63.
4. Faga MG, Guicciardi S, Esposito L, Bellosi A, Pezzotti G. Alumina/alumina and alumina–zirconia/alumina–zirconia joints through glass interlayers, microstructure, mechanical properties and residual stresses. *Adv Eng Mater* 2005;**7**:535–40.

5. Isgrò G, Wang H, Kleverlaan CJ, Feilzer AJ. The effects of thermal mismatch and fabrication procedures on the deflection of layered all-ceramic discs. *Dent Mater* 2005;**21**:649–55.
6. DeHoff PH, Barrett AA, Lee RB, Anusavice KJ. Thermal compatibility of dental ceramic systems using cylindrical and spherical geometries. *Dent Mater* 2008;**24**:744–52.
7. Hermann I, Bhowmick S, Lawn BR. Role of core support material in veneer failure of brittle layer structures. *J Biomed Mater* 2007;**82B**:115–21.
8. Fleming GJP, El-Lakwah SFA, Harris JJ, Marquis PM. The effect of core: dentin thickness ratio on the bi-axial flexure strength and fracture mode and origin of bilayer dental ceramic composites. *Dent Mater* 2005;**21**:164–72.
9. Thompson GA. Influence of relative layer height and testing method on the failure mode and origin in a bilayer dental ceramic composite. *Dent Mater* 2000;**16**:235–43.
10. White SN, Miklus VG, McLaren EA, Lang LA, Caputo AA. Flexural strength of a layered zirconia and porcelain dental all-ceramic system. *J Prosthet Dent* 2005;**94**:125–31.
11. Isgrò G, Pallav P, Van der Zel JM, Feilzer AJ. The influence of the veneering porcelain and different surface treatments on the biaxial flexural strength of a heat-pressed ceramic. *J Prosthet Dent* 2003;**90**:465–73.
12. Aboushelib MN, Jager N, Kleverlaan CJ, Feilzer AJ. Effect of loading method on the fracture mechanics of two layered all-ceramic restorative systems. *Dent Mater* 2007;**23**:952–9.
13. Lawn BR. *Fracture of Brittle Solids*. Cambridge: Cambridge University Press; 1993.
14. Guazzato M, Proos K, Quach L, Swain MV. Strength, reliability and mode of fracture of bilayer porcelain/zirconia (Y-TZP) dental ceramics. *Biomaterials* 2004;**25**:5045–52.
15. Imanishi A, Nakamura T, Ohyama T. 3D Finite element analysis of all-ceramic posterior crowns. *J Oral Rehabil* 2003;**30**:818–22.
16. Kou W, Kou S, Liu H, Sjögren G. Numerical modeling of the fracture process in a three-unit all-ceramic fixed partial denture. *Dent Mater* 2007;**23**:1042–9.
17. Lin P, Wong Robina HC, Chau KT, Tang CA. Multi-crack coalescence in rock-like material under uniaxial and biaxial loading. *Key Eng Mater* 2000;**183–187**:809–14.
18. Wang DG, Yang JY, Li LC, Jiang W. Numerical simulation of short cracks in fiber-reinforced ceramics. *Key Eng Mater* 2006;**324–325**:947–50.
19. Sheppard LM, Ketron L, editors. *Ceramic Source'90, vol. 5. Technical Data. Annual Source Book*. Amer. Ceram. Soc. Inc.; 1990.
20. Cui J, Chen YF, Chao YL, Chen CX, Ou J, Sui L, Zhang WQ. Bi-axial flexure strength, weibull modulus and fracture mode of alumina glass-infiltrated core/veneer ceramic composites. *Key Eng Mater* 2007;**353–358**:1556–9.
21. Kondo N, Suzuki Y, Ohji T. Super plastic sinter-forging of silicon nitride with anisotropic microstructure formation. *J Am Ceram Soc* 1999;**82**:1067–9.
22. Schneider SJ, editor. *Engineered Materials Handbook, vol. 4, Ceramics and Glasses*. Materials Park, OH: ASM International; 1991.
23. Hsueh CH, Thompson GA, Jadaan OM, Wereszczak AA, Becher PF. Analyses of layer-thickness effects in bilayer dental ceramics subjected to thermal stresses and ring-on-ring tests. *Dent Mater* 2008;**24**:9–17.
24. Lawn B, Bhowmick S, Bush MB, Qasim T, Rekow ED, Zhang Y. Failure modes in ceramic-based layer structures: a basis for materials. *J Am Ceram Soc* 2007;**90**:1671–83.
25. Hermnn I, Bhowmick S. Competing fracture modes in brittle materials subject to concentrated cyclic loading in liquid environments: trilayer structures. *J Mater Res* 2006;**21**:512–21.